Inorganic Chemistry

Article

pubs.acs.org/IC

High-Voltage Cathode Materials for Lithium-Ion Batteries: Freeze-Dried $LiMn_{0.8}Fe_{0.1}M_{0.1}PO_4/C$ (M = Fe, Co, Ni, Cu) Nanocomposites

Amaia Iturrondobeitia,[†,‡] Aintzane Goñi,[†,§] Izaskun Gil de Muro,[†,§] Luis Lezama,[†,§] Chunjoong Kim,[∥] Marca Doeff,[⊥] Jordi Cabana,[∥] and Teófilo Rojo*[,†,‡]

[†]Departamento de Química Inorgánica, Universidad del País Vasco UPV/EHU, P.O. Box 644, 48080 Bilbao, Spain

[‡]Parque Tecnológico de Álava, CIC energiGUNE. Albert Einstein 48, 01510 Miñano, Álava Spain

[§]Parque Científico y Tecnológico de Bizkaia, BCMaterials, Ibaizabal Bidea 500, 48160 Derio, Spain

[∥]Department of Chemistry, University of Illinois at Chicago, Chicago, Illinois 60607, United States

[⊥]Environmental Energy Technologies Division, Lawrence Berkeley National Laboratory, 1 Cyclotron Road, MS62R0203, Berkeley, California 94720-8168, United States

ABSTRACT: Four $LiMn_{0.8}Fe_{0.1}M_{0.1}PO_4/C$ (M = Fe, Co, Ni, Cu) cathode materials have been synthesized via a freeze-drying method. The samples have been characterized by powder X-ray diffraction, transmission electron microscopy, magnetic susceptibility, and electrochemical measurements. The composition and effective insertion of the transition-metal substituents in $LiMnPO_4$ have been corroborated by elemental analysis, the evolution of the crystallographic parameters, and the magnetic properties. The morphological characterization of the composites has demonstrated that the phosphate nanoparticles are enclosed in a matrix of amorphous carbon. Among them, $LiMn_{0.8}Fe_{0.1}Ni_{0.1}PO_4/C$ is the most promising cathode material, providing a good electrochemical performance in all aspects: high voltage and specific capacity values, excellent cyclability, and good rate capability. This result has been attributed to several factors, such as the suitable morphology of the sample, the good connection afforded by the in situ generated carbon, and the amelioration of the structural stress provided by the presence of Ni^{2+} and Fe^{2+} in the olivine structure.

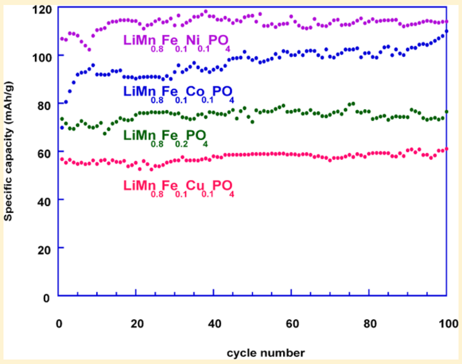

■ INTRODUCTION

Olivine-type $LiMPO_4$ (M = Mn, Fe, Co, Ni) are among the most technologically relevant cathode materials for lithium-ion batteries.[1−10] $LiFePO_4$ is the most prominent phase because of its high specific capacity, excellent thermal stability, low cost, and environmental friendliness.[11,12] However, its fairly low reaction voltage (3.4 V vs Li^+/Li) affords less energy density than that required for the next generation of energy storage devices.[13,14] $LiCoPO_4$ and $LiNiPO_4$ present higher reaction voltages, 4.8 and 5.1 V, respectively. Although this results in higher theoretical energy densities, those high potentials put the stability of the electrolytic solutions at risk.[15] $LiMnPO_4$ reacts at 4.1 V versus Li^+/Li, providing a ~20% higher energy density than that of $LiFePO_4$.[16] Unfortunately, the electronic and ionic conductivity of $LiMnPO_4$ is insufficient for good electrochemical performance. In addition, manganese phosphate also presents other disadvantages, such as the structural instability generated by the volume change between the lithiated and delithiated phases of the electrochemical couple, $LiMnPO_4$ and $MnPO_4$, and the Jahn−Teller distortion of Mn^{3+}.[17,18] Several investigations have been directed toward improving the electrochemical response of $LiMnPO_4$.[19−24] The most widespread solutions are reduction of the particle size to nanometric scale,[25,26] surface coating by an electronic conductor,[27,28] or structural substitution by small amounts of metallic cations.[29−32] Coating with carbon also resulted in improvements by providing a good connection between the active particles.[33] In addition, recent studies have shown that mixing metals in $LiMnPO_4$ extends the solid solution domains during transformation to $MnPO_4$, which reduces the strain during cycling.[34] The $LiMn_{1-x}Fe_xPO_4$ ($x = 0.1−0.2$) solid solution has shown a better electrochemical response at different C rates,[35] while preserving at least some of the characteristic discharge capacity at 4.1 V,[36−41] typical of $LiMnPO_4$. Moreover, the modification could also ameliorate the structural stress caused by the Jahn−Teller effect of Mn^{3+}. In this sense, transition-metal ions, such as Fe^{2+}, Co^{2+}, Ni^{2+}, or Cu^{2+}, are good candidates for substitution because they are able to occupy the same crystallographic position as Mn^{2+} because of their similar crystal−chemical properties.[42−45] In this work, nanosizing, carbon coating, and substitution have been combined in order to produce new and better-performing cathode materials based on $Li(Mn_{0.8}Fe_{0.1}M_{0.1})PO_4/C$ (M = Fe, Co, Ni, Cu) composites. We report on the synthesis and morphological, magnetic, and electrochemical characterization of four different samples,

Received: November 26, 2014
Published: February 27, 2015

DOI: 10.1021/ic5028306
Inorg. Chem. 2015, 54, 2671−2678

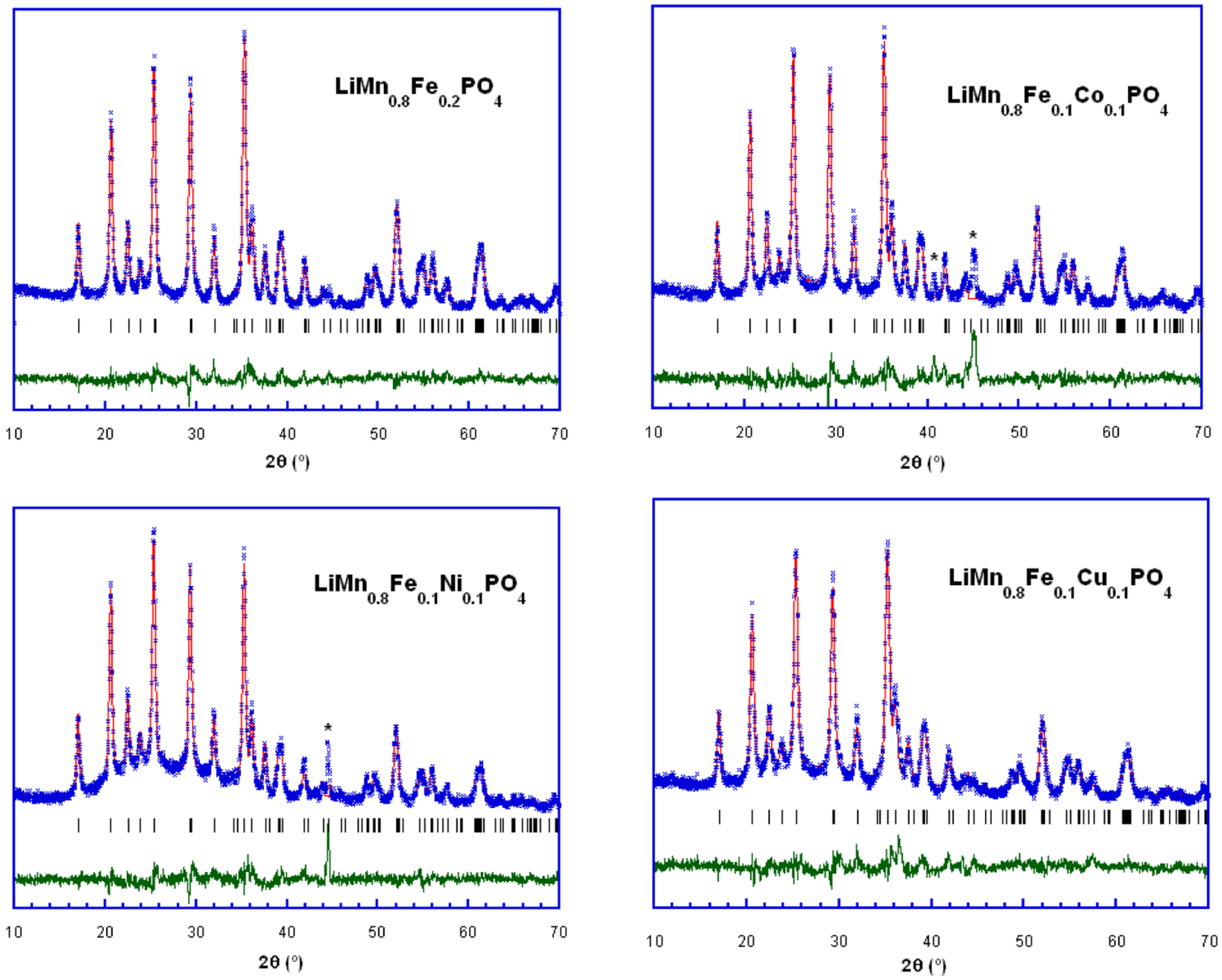

Figure 1. Rietveld refinement patterns of the XRD data for the $LiMn_{0.8}Fe_{0.1}M_{0.1}PO_4/C$ (M = Fe, Co, Ni, Cu) samples. Asterisks indicate reflections corresponding to impurities.

establishing correlations between the composition and electrochemical performance.

■ EXPERIMENTAL SECTION

Materials and Reagents. The following materials and reagents were used as purchased without further purification: citric acid monohydrate (99.5%, Sigma-Aldrich), manganese(III) acetate dihydrate (97%, Sigma-Aldrich), iron(II) acetate (95%, Sigma-Aldrich), nickel(II) acetate tetrahydrate (98%, Sigma-Aldrich), cobalt(III) acetate tetrahydrate (98%, Sigma-Aldrich), and lithium hydroxide monohydrate (99%, Fluka).

Sample Preparation. The $LiMn_{0.8}Fe_{0.1}M_{0.1}PO_4/C$ (M = Fe, Co, Ni, Cu) samples were synthesized using a freeze-drying method.[46] First, $C_6H_8O_7{\cdot}H_2O$, $Mn(C_2H_3O_2)_3{\cdot}2H_2O$, $LiOH{\cdot}H_2O$, $NH_4H_2PO_4$, and, depending on the substituent, $Fe(C_2H_3O_2)_2$, $Co(C_2H_3O_2)_2{\cdot}4H_2O$, $Ni(C_2H_3O_2)_2{\cdot}4H_2O$, or $Cu(C_2H_3O_2)_2{\cdot}H_2O$, were dissolved in 25 mL of H_2O in stoichiometric molar ratios. The resultant solutions were subsequently frozen in round-bottom flasks that contained liquid nitrogen. Afterward, the round-bottom flasks were connected to the freeze dryer for 48 h at a pressure of 3×10^{-1} mbar and a temperature of −80 °C to sublime the solvent. The as-obtained precursors were subjected to a first heat treatment at 350 °C for 3 h under a N_2 atmosphere. Subsequently, the products were ball-milled for 30 min, and then they were calcined at 700 °C for 6 h under $N_2(g)$. This procedure led to four powder samples: $LiMn_{0.8}Fe_{0.2}PO_4/C$, $LiMn_{0.8}Fe_{0.1}Co_{0.1}PO_4/C$, $LiMn_{0.8}Fe_{0.1}Ni_{0.1}PO_4/C$, and $LiMn_{0.8}Fe_{0.1}Cu_{0.1}PO_4/C$, which were further characterized.

Characterization. Elemental analysis of the samples was performed in a Eurovector 3000 instrument. Powder X-ray diffraction (XRD) patterns were collected in a Bruker D8 Advance Vario diffractometer using Cu Kα radiation at room temperature. The obtained diffraction data were refined by Rietveld analysis using the *FullProf* program.[47] Morphological characterization was carried out by transmission electron microscopy (TEM) using a Philips CM200 microscope equipped with an EDAX energy-dispersive X-ray analyzer. Magnetic measurements were carried out in a SQUID magnetometer from 5 K to room temperature under a 0.1 T magnetic field. A total of 2032 coin cells were assembled to evaluate the electrochemical performance of the samples. To prepare the electrodes, the active materials were mixed with conducting carbon black (Super P, Timcal) and a poly(vinylidene fluoride) binder with a weight ratio of 80:10:10 and dispersed in *N*-methyl-2-pyrrolidone to form a slurry. The slurry was then cast onto aluminum current collectors and dried at 120 °C in a vacuum oven overnight. Electrochemical cells with metallic lithium foil as the counter electrode, Celgard 2400 polypropylene separators, and 1 M $LiPF_6$ in 50:50 ethylene carbonate/dimethyl carbonate as the electrolytic solution were assembled in an argon-filled glovebox. All of the electrochemical measurements were carried out on a Bio-Logic VMP3 potentiostat/galvanostat at room temperature. Typical electrode loadings were 1.3 mg/cm^2. The galvanostatic charge−discharge experiments were performed between 2.5 and 4.4 V at a current rate equivalent to 0.04*C* or 1*C*, in which the *C* rate is defined as discharging the full capacity (approximately 170 mAh/g for the active material) in 1 h. For some cells, CCCV charging was used: once the voltage limit of 4.4 was reached galvanostatically, a constant voltage step was used until the

Table 1. Results of Structure Analysis Calculated from XRD Rietveld Refinement of $LiMn_{0.8}Fe_{0.2}PO_4$, $LiMn_{0.8}Fe_{0.1}Co_{0.1}PO_4$, $LiMn_{0.8}Fe_{0.1}Ni_{0.1}PO_4$, and $LiMn_{0.8}Fe_{0.1}Cu_{0.1}PO_4$

$LiMPO_4$ (space group *Pnma*)			$Mn_{0.8}Fe_{0.2}$	$Mn_{0.8}Fe_{0.1}Co_{0.1}$	$Mn_{0.8}Fe_{0.1}Ni_{0.1}$	$Mn_{0.8}Fe_{0.1}Cu_{0.1}$
cell parameters (Å)	*a*		10.420(1)	10.428(2)	10.413(1)	10.430(1)
	b		6.0883(6)	6.0976(1)	6.0903(6)	6.0959(9)
	c		4.7340(5)	4.7329(9)	4.7383(7)	4.7369(8)
	volume ($Å^3$)		300.33(5)	300.94(9)	300.50(6)	301.18(9)
fractional atomic coordinates	Li	*x*	0.0000	0.0000	0.0000	0.0000
		y	0.0000	0.0000	0.0000	0.0000
		z	0.0000	0.0000	0.0000	0.0000
	M	*x*	0.2805(2)	0.2814(3)	0.2821(3)	0.2808(4)
		y	0.2500	0.2500	0.2500	0.2500
		z	0.969(1)	0.964(1)	0.968(1)	0.966(1)
	P	*x*	0.0952(6)	0.0973(8)	0.093(1)	0.100(1)
		y	0.2500	0.2500	0.2500	0.2500
		z	0.408(1)	0.405(2)	0.387(2)	0.408(3)
	O1	*x*	0.092(1)	0.093(2)	0.105(1)	0.086(2)
		y	0.2500	0.2500	0.2500	0.2500
		z	0.714(3)	0.705(5)	0.693(3)	0.693(6)
	O2	*x*	0.455(1)	0.458(2)	0.461(2)	0.449(2)
		y	0.2500	0.2500	0.2500	0.2500
		z	0.224(2)	0.228(2)	0.213(2)	0.236(3)
	O3	*x*	0.1552(8)	0.154(1)	0.156(1)	0.148(1)
		y	0.049(1)	0.040(1)	0.046(2)	0.039(3)
		z	0.265(1)	0.263(2)	0.272(2)	0.244(2)
reliability factors	χ^2		2.33	2.22	1.93	2.63
	R_p (%)		6.82	6.15	4.85	6.02
	R_{wp} (%)		8.94	7.78	6.28	7.63
	R_f (%)		7.44	5.84	6.34	12.1

Table 2. Selected Bond Lengths (Å) Obtained from XRD Rietveld Refinement of $LiMn_{0.8}Fe_{0.2}PO_4$, $LiMn_{0.8}Fe_{0.1}Co_{0.1}PO_4$, $LiMn_{0.8}Fe_{0.1}Ni_{0.1}PO_4$, and $LiMn_{0.8}Fe_{0.1}Cu_{0.1}PO_4$

$LiMPO_4$	Mn[a]	$Mn_{0.8}Fe_{0.2}$	$Mn_{0.8}Fe_{0.1}Co_{0.1}$	$Mn_{0.8}Fe_{0.1}Ni_{0.1}$	$Mn_{0.8}Fe_{0.1}Cu_{0.1}$
Li−O1	2.2301(2)	2.254(11)	2.285(17)	2.373(11)	2.294(20)
Li−O2	2.0823(2)	2.059(6)	2.042(7)	2.081(7)	2.042(10)
Li−O3	2.0758(2)	2.068(8)	2.048(10)	2.091(9)	1.944(12)
Mn−O1	2.2463(3)	2.300(16)	2.312(21)	2.259(15)	2.401(24)
Mn−O2	2.1600(3)	2.184(13)	2.227(16)	2.194(19)	2.170(15)
Mn−O3	2.1625(2)	2.173(8)	2.120(10)	2.131(11)	2.183(17)
Mn−O3′	2.2420(3)	2.267(8)	2.323(11)	2.309(11)	2.302(15)

[a] Data corresponding to $LiMnPO_4$ are extracted from ref 50.

current fell to a value of 0.01*C*, to ensure full charging of the samples. The rate capability of the materials was characterized through the acquisition of a "signature curve" (SC)[48] obtained by a protocol that consists of an initial charge performed at 0.04*C*, followed by a series of successive discharges at different rates, from the highest (1*C*) to the lowest (0.01*C*), with relaxation periods of 5 min and no charging step in between. The cumulative capacity at each rate was used to construct modified Peukert plots. To calculate the capacity values, the weight of only $LiMn_{0.8}Fe_{0.1}M_{0.1}PO_4$ (M = Fe, Co, Ni, Cu) was considered, not including the in situ carbon.

■ RESULTS AND DISCUSSION

Elemental analysis of the four freeze-dried samples, $LiMn_{0.8}Fe_{0.2}PO_4/C$, $LiMn_{0.8}Fe_{0.1}Co_{0.1}PO_4/C$, $LiMn_{0.8}Fe_{0.1}Ni_{0.1}PO_4/C$, and $LiMn_{0.8}Fe_{0.1}Cu_{0.1}PO_4/C$, showed that the percentage of carbon was close to 27 wt % for all of the composites because of the similar synthesis procedures used, specifically the same amount of organic matter in the precursor mixtures. Selection of the amount of the carbon source was carried out considering our previous results about the influence of the carbon content on $LiFePO_4/C$ samples synthesized by the freeze-drying process.[49]

The materials were characterized by powder XRD. The $LiMn_{0.8}Fe_{0.1}M_{0.1}PO_4/C$ samples presented diffraction patterns very similar to that corresponding to the parent olivine $LiMnPO_4$. All of the diffraction peaks were indexed to the orthorhombic *Pnma* space group (Figure 1). No peaks corresponding to carbon were observed. For $LiMn_{0.8}Fe_{0.1}Co_{0.1}PO_4/C$ and $LiMn_{0.8}Fe_{0.1}Ni_{0.1}PO_4/C$, two additional weak diffraction maxima were detected at around $2\theta \approx 45°$. These reflections, marked with asterisks in Figure 1, could be attributed to some ferrite-type compounds, such as $CoFe_2O_4$ (PDF card 79-1744), $MnFe_2O_4$ (PDF card 74-2103), or $NiFe_2O_4$ (PDF card 86-2267). However, the composition of those ferrites is not easy to determine. In MM'_2O_4, both positions M and M′ can be occupied by any of Mn, Fe, Co, Ni, or Cu or by a mixture of them, resulting in a wide variety of phases. Therefore, it is difficult to reach an accurate result for the amount of impurities using the *Fullprof* software. Thus, the regions of the diffraction patterns with any peak of impurities have been excluded from the refinement. Considering that all materials have been prepared following the same synthesis procedure, it is not unreasonable to suspect that all of the samples could contain small amounts of ferrite impurities below the detection limit.

The structural parameters for the four $LiMn_{0.8}Fe_{0.1}M_{0.1}PO_4/C$ (M = Fe, Co, Ni, Cu) samples were refined by Rietveld analysis. Only the diffraction peaks of the olivine phases have been considered for the crystallographic study. Figure 1 shows the experimental, calculated, and difference XRD patterns. The refined cell parameters and fractional atomic coordinates, together with the reliability factors reached, are listed in Table 1. Selected bond distances are shown in Table 2. The data corresponding to pure $LiMnPO_4$[50] have also been included for comparison.

In all cases, the structural parameters show deviations compared to those of pure $LiMnPO_4$ (as shown in Table 1). It implies that the substituted elements are effectively located in the olivine structure, resulting in a solid solution instead of a mixture. The evolution of the cell volume values with the ionic radii of various dopant elements is difficult to relate. Rietveld refinement further reveals deviations of the bond lengths in the crystal structure of $LiMnPO_4$ by transition-metal substitutions (see Table 2). The Li−O mean distance for Ni-substituted phosphate (2.182 Å) is lengthened compared to that of 2.129 Å in pure $LiMnPO_4$. For the other compounds, $LiMn_{0.8}Fe_{0.2}PO_4$, $LiMn_{0.8}Fe_{0.1}Co_{0.1}PO_4$, and $LiMn_{0.8}Fe_{0.1}Cu_{0.1}PO_4$, the Li−O average distances are similar or shorter.

The average Mn−O bond lengths in the MnO_6 octahedra also exhibit noticeable changes for all of the $LiMn_{0.8}Fe_{0.1}M_{0.1}PO_4/C$ samples. The majority of the Mn−O bonds become longer than those observed for $LiMnPO_4$, except Mn−O3 (Figure 2) in $LiMn_{0.8}Fe_{0.1}Co_{0.1}PO_4$ and $LiMn_{0.8}Fe_{0.1}Ni_{0.1}PO_4$, which shrink. In $LiMnPO_4$, during the oxidation of Mn^{2+} to Mn^{3+} giving rise to $MnPO_4$, the metal−oxygen bonds change significantly: Mn−O3 is reduced while Mn−O3′ is elongated due to Jahn−Teller distortion.[51] The substitution of Ni and Co in the $LiMn_{0.8}Fe_{0.1}M_{0.1}PO_4$ phosphates results in a similar structural distortion. Therefore, a better accommodation of the Mn^{3+} ions in the framework can be expected for those phases on delithiation.

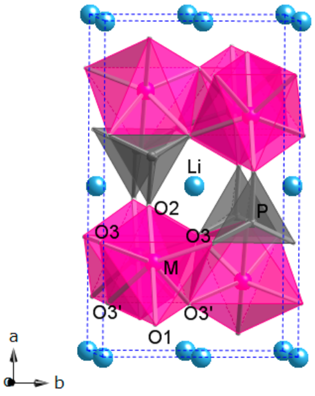

Figure 2. Crystal structure of the $LiMPO_4$ olivine compounds.

The average particle size of the samples was calculated using Scherrer's equation (eq 1):

$$D = \frac{K\lambda}{B_{fwhm}\cos\theta} \qquad (1)$$

where K is a dimensionless shape factor, B is the line broadening at half the maximum intensity, λ is the X-ray wavelength, and θ is the Bragg angle. For all of the composites, the average crystallite size was estimated to be ∼30 nm by fitting (121) peaks. The morphologies of the four freeze-dried composites were also further examined by TEM. Figure 3 shows the selected micrographs corresponding to $LiMn_{0.8}Fe_{0.2}PO_4/C$ (Figure 3a,c) and $LiMn_{0.8}Fe_{0.1}Ni_{0.1}PO_4/C$ (Figure 3b,d) as examples. The images are representative of all of the materials, as expected from the fact that the synthetic conditions were the same. The samples were constituted of aggregates of nanosized phosphate particles and amorphous carbon. The phosphate crystal size ranged between 20 and 40 nm, and they were embedded inside the in situ generated carbonaceous web. That amorphous coating complicated a better inspection of the morphology. The carbon matrix inhibited growth of the olivine particles; this type of composite with a homogeneous distribution of phosphate nanoparticles is typical of the freeze-drying process.

Magnetic susceptibility measurements were carried out in the 5−300 K temperature range at 1 kOe. Figure 4 shows thermal evolution of the molar magnetic susceptibility obtained for field-cooled (FC) and zero-field-cooled (ZFC) $LiMn_{0.8}Fe_{0.2}PO_4/C$ and $LiMn_{0.8}Fe_{0.1}Co_{0.1}PO_4/C$ samples, as representative examples of the series of compounds studied here. In all cases, as the temperature decreased, the magnetic susceptibility (χ_m) rose, reaching a maximum. At that point (Neél temperature, T_N), the magnetic behavior exhibited a transition to antiferromagnetic ordering, which is typical of olivine $LiMPO_4$.[52] However, for each compound studied, the χ_m maximum was located at a different T_N values. The inset in Figure 4 represents the ordering temperatures that have been observed for each composite, together with the characteristic T_N values corresponding to the $LiMPO_4$ (M = Mn, Fe, Co, Ni) parent phases. As far as we are aware, up to now, olivine-type $LiCuPO_4$ remains unknown, and its virtual T_N is not available. Variation of T_N as a function of the inserted transition metal follows the trend of the parent compounds. This is further evidence of the effective insertion of at least a part of the different substituents in the $LiMnPO_4$ phase.

Although the antiferromagnetic interactions in the samples are predominant, the FC and ZFC curves diverged from room temperature, which is indicative of the existence of an additional ferrimagnetic phase. The impurity stays magnetically ordered above room temperature. This type of magnetic behavior is in accordance with the presence of small amounts of ferrite phases, such as $MnFe_2O_4$, $CoFe_2O_4$, or $NiFe_2O_4$ detected in some of the XRD patterns. The divergence between the FC and ZFC curves is more noticeable for $LiMn_{0.8}Fe_{0.1}Co_{0.1}PO_4/C$ and $LiMn_{0.8}Fe_{0.1}Cu_{0.1}PO_4/C$ than for the other composites. This suggests that these two composites probably contain larger amounts of ferrimagnetic secondary phases. A very small quantity of any ferrite is needed for detection of its magnetic signal, especially considering the weak magnetic behavior of the phosphates.

To evaluate the electrochemical performance, lithium half-cells containing $LiMn_{0.8}Fe_{0.1}M_{0.1}PO_4/C$ composites were charged and discharged at currents corresponding to $C/25$ and $1C$. Figure 5 shows the first charge−discharge profiles of the samples at $C/25$ at room temperature. It is interesting to note that some of the profiles have two voltage plateaus at approximately 4.1 and 3.5 V corresponding to the Mn^{3+}/Mn^{2+} and Fe^{3+}/Fe^{2+} redox pairs, respectively. The plateau at 3.5 V is

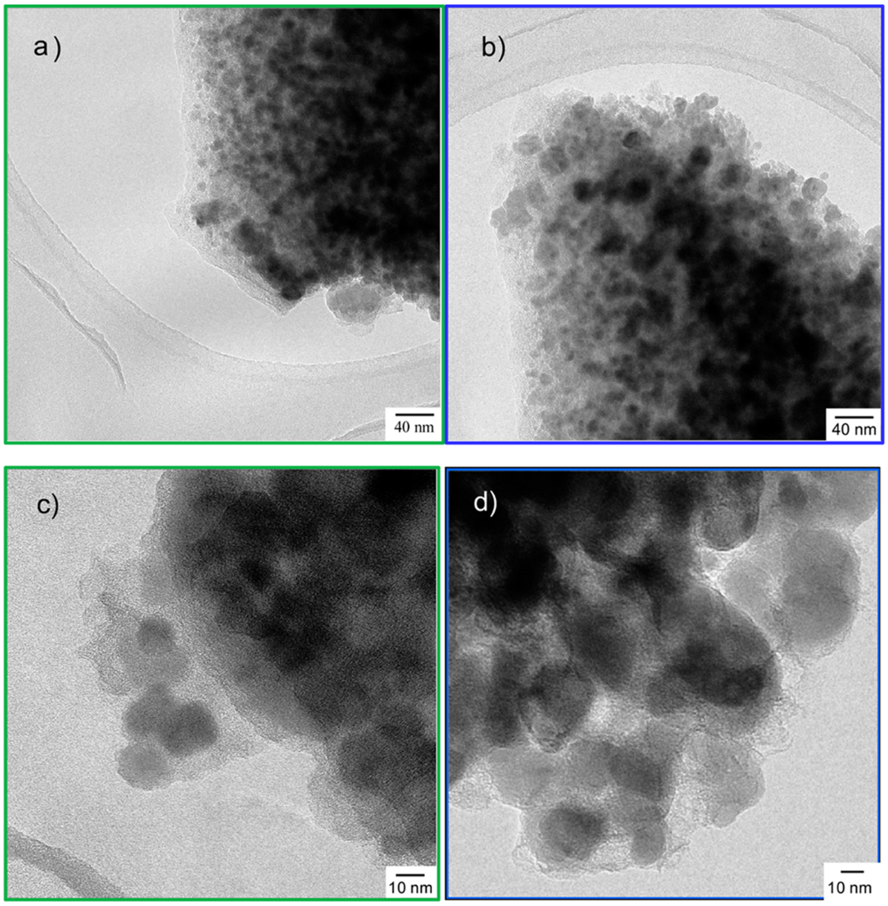

Figure 3. Representative TEM micrographs corresponding to (a) $LiMn_{0.8}Fe_{0.2}PO_4/C$, (b) $LiMn_{0.8}Fe_{0.1}Ni_{0.1}PO_4/C$, (c) magnification of $LiMn_{0.8}Fe_{0.2}PO_4/C$, and (d) magnification of $LiMn_{0.8}Fe_{0.1}Ni_{0.1}PO_4/C$.

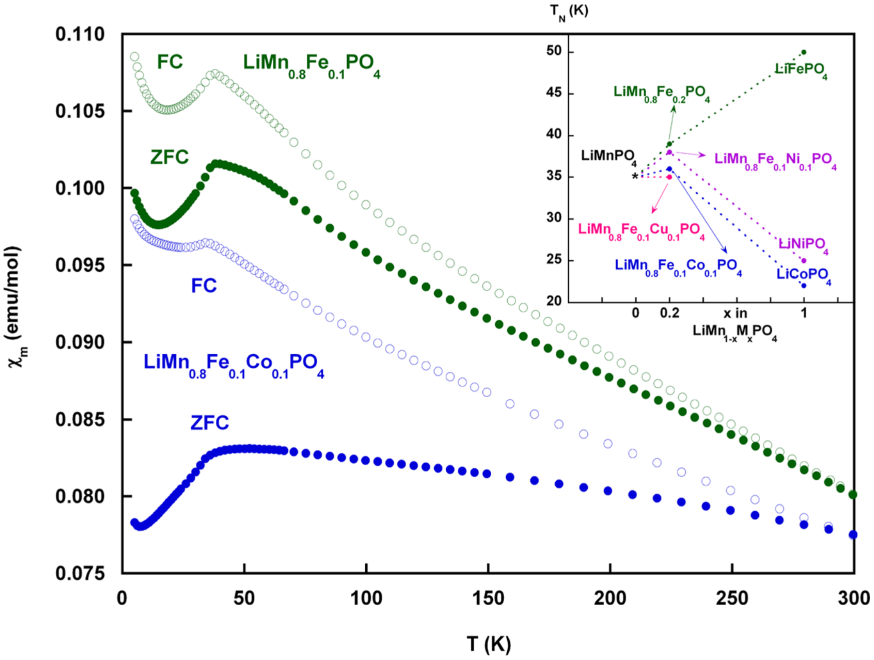

Figure 4. Thermal evolution of the molar magnetic susceptibility curves obtained for $LiMn_{0.8}Fe_{0.2}PO_4/C$ (in green) and $LiMn_{0.8}Fe_{0.1}Co_{0.1}PO_4/C$ (in blue). Inset: Magnetic ordering temperatures of the different $LiMn_{0.8}Fe_{0.1}M_{0.1}PO_4$ (M = Fe, Co, Ni, Cu) compounds together with the characteristic T_N values corresponding to the $LiMPO_4$ (M = Mn, Fe, Co, Ni) parent phases.

more perceptible for the $LiMn_{0.8}Fe_{0.2}PO_4/C$ composite, as could be expected from its higher content in iron.

The initial specific discharge capacity of $LiMn_{0.8}Fe_{0.2}PO_4/C$ was quite low, 68 mAh/g. The lithium-ion extraction depth in the

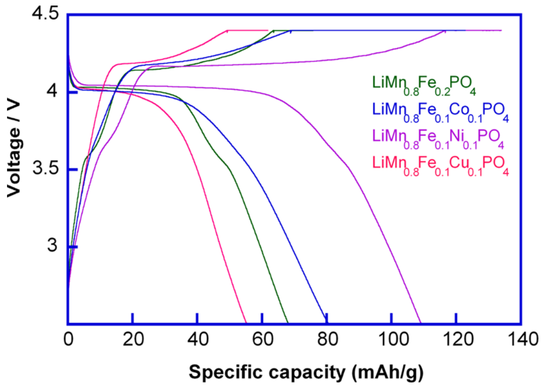

Figure 5. First charge−discharge profiles of the $LiMn_{0.8}Fe_{0.1}M_{0.1}PO_4/C$ (M = Fe, Co, Ni, Cu) composites at *C*/25 at room temperature.

first charge would be pertinent to getting $Li_{0.6}Mn_{0.8}Fe_{0.2}PO_4$. However, the replacement of 0.1 mol of Fe^{2+} with Ni^{2+} increased the capacity value to 110 mAh/g, which indicates a previously deeper lithium extraction on charge until $Li_{0.35}Mn_{0.8}Fe_{0.1}Ni_{0.1}PO_4$. Substitution with Co^{2+} caused a moderate increase of the capacity to 80 mAh/g. Taking into account that the morphology of all of these composites is very similar, and consequently the surface area and carbon content are equivalent, the improvement of the electrochemical response might be attributed to the presence of Ni^{2+} and Co^{2+} in the olivine structure. In contrast, the presence of Cu^{2+} decreased the specific capacity to 57 mAh/g. This fact could be related to the absence of a stable $LiCuPO_4$ olivine phase. On the basis of these results, the $LiMn_{0.8}Fe_{0.1}Ni_{0.1}PO_4/C$ composite offers the best specific capacity with the lowest polarization. In contrast, $LiMn_{0.8}Fe_{0.1}Cu_{0.1}PO_4/C$ is the most polarized cathode material, and it provides the smallest capacity for energy storage.

The cycling performance of the four tested cathode materials is shown in Figure 6. After 100 cycles at *C*/25, the capacity retention for all compounds was close to 100%. In addition, for $LiMn_{0.8}Fe_{0.1}Ni_{0.1}PO_4/C$, and especially for $LiMn_{0.8}Fe_{0.1}Co_{0.1}PO_4/C$, a progressive improvement of the specific capacity is observed as the cycle number goes up. This fact could probably be ascribed to the better wetting of the active material with the electrolyte as the coating develops cracks and pores upon cycling.

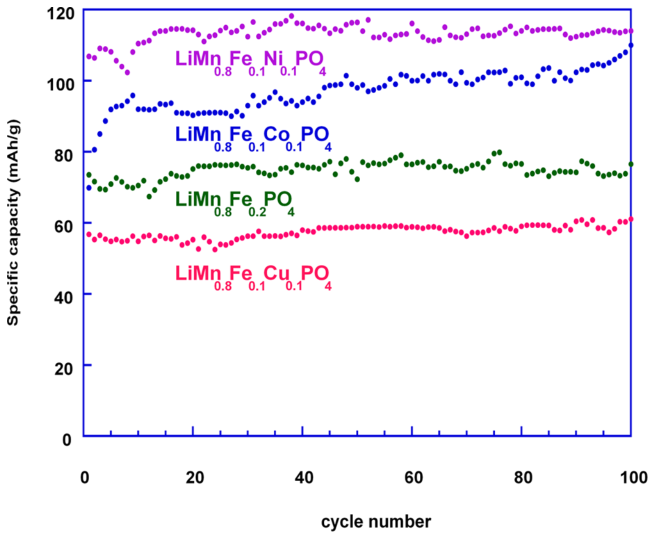

Figure 6. Cycling performance of the four tested $LiMn_{0.8}Fe_{0.1}M_{0.1}PO_4/C$ (M = Fe, Co, Ni, Cu) cathode materials at *C*/25.

The rate capability of the samples was evaluated using SCs as described in refs46 and 53. Cells were first charged to 4.3 V at 0.04*C* and discharged to 3.5 V at different rates, starting with the highest one (1*C*) and finishing with the slowest one (0.01*C*). A relaxation period of 5 min was taken after each discharge step, without charging in between. The cumulative charge passed at each rate was considered as the capacity value for the given rate. Figure 7, which shows the modified Peukert plots, indicates that $LiMn_{0.8}Fe_{0.1}Ni_{0.1}PO_4/C$ had the best performance, maintaining 95% of the initial specific capacity at 1*C*. $LiMn_{0.8}Fe_{0.2}PO_4/C$ and $LiMn_{0.8}Fe_{0.1}Co_{0.1}PO_4/C$ exhibited a similar behavior between each other, retaining 93% of the specific capacity at 1*C*. In contrast, $LiMn_{0.8}Fe_{0.1}Cu_{0.1}PO_4/C$ displayed the poorest rate capability response at 1*C* because the capacity retention was only 85%.

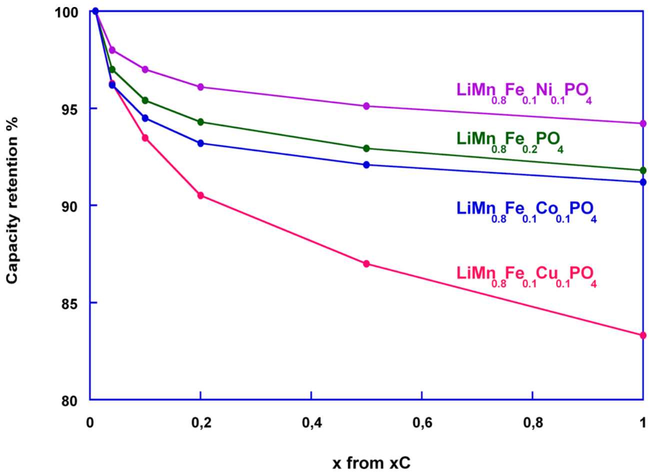

Figure 7. Modified Peukert plot for cells containing the four $LiMn_{0.8}Fe_{0.1}M_{0.1}PO_4/C$ (M = Fe, Co, Ni, Cu) cathode materials.

On the basis of these results, $LiMn_{0.8}Fe_{0.1}Ni_{0.1}PO_4/C$ is the most promising cathode material of the formulations in this study, providing a good electrochemical performance in all aspects: high specific capacity values, excellent cyclability, and good rate capability. One of the most important reasons is that the freeze-drying synthesis method promotes the formation of a nanometric phosphate/carbon composite material with a morphology that provides good electronic and ionic connections between active material particles. In particular, the in situ generated carbon matrix supplies the necessary connection and cohesion between the active nanoparticles. The presence of a small amount of Ni^{2+} in the olivine phosphate provides structural stability accommodating the volume change between the $LiMnPO_4$ and $MnPO_4$ phases, favoring the redox exchange and the extraction−insertion of lithium ions. Moreover, relatively longer Li−O bonds with smaller binding energy would lead to an easier migration of Li^+ cations during the charge−discharge processes. These reasons would explain the improved electrochemical performance of the $LiMn_{0.8}Fe_{0.1}Ni_{0.1}PO_4/C$ composite.

■ CONCLUSIONS

The freeze-drying method is a useful synthetic procedure for obtaining nanosized $LiMn_{0.8}Fe_{0.1}M_{0.1}PO_4/C$ (M = Fe, Co, Ni, Cu) composites, which can be used as cathode materials. The predominant phase in all cases was the orthorhombic olivine structure (*Pnma* space group), although small amounts of ferrite-type impurities were detected in some cases. Variation of the crystallographic parameters agreed with the changes in the composition, providing verification that solid solutions were produced. The morphological study demonstrated that the phosphate nanoparticles are enclosed in a matrix of amorphous carbon in the composite materials. The magnetic characterization corroborated the effective insertion of dopants in the $LiMn_{0.8}Fe_{0.1}M_{0.1}PO_4$ (M = Fe, Co, Ni, Cu) phases because each compound presented its own characteristic ordering temperature. The electrochemical study revealed that the cosubstitution of small amounts of Fe^{2+} and Ni^{2+} into $LiMnPO_4$ enhances the electrochemical performance. The $LiMn_{0.8}Fe_{0.1}Ni_{0.1}PO_4$/C material showed the best performance in all aspects: high specific capacity, excellent cyclability, and good rate capability. This result has been attributed to several factors, such as the suitable morphology of the sample, the good connection that provides the in situ generated carbon, and the amelioration of the structural stress in the olivine structure during the cycling process. Thus, the good electrochemical performance and high discharge potential (4.1 V) of the $LiMn_{0.8}Fe_{0.1}Ni_{0.1}PO_4$/C composite make it a promising cathode material for lithium-ion batteries.

■ AUTHOR INFORMATION

Corresponding Author

*E-mail: trojo@cicenergigune.com. Tel: +34945 297 108.

Author Contributions

The manuscript was written through contributions of all authors. All authors have given approval to the final version of the manuscript.

Notes

The authors declare no competing financial interest.

■ ACKNOWLEDGMENTS

This work was financially supported by the Ministerio de Educación y Ciencia (Grant MAT2013-41128-R), the Universidad del Pais Vasco/Euskal Herriko Unibertsitatea, and the Gobierno Vasco/Eusko Jaurlaritza (IT570-13, Etortek CIC EnergiGUNE 10). A.I. thanks the Gobierno Vasco/Eusko Jaurlaritza for a fellowship. Portions of this work were supported by the Assistant Secretary for Energy Efficiency and Renewable Energy, Office of Vehicle Technologies, of the U.S. Department of Energy under Contract DE-AC02-05CH11231 under the Batteries for Advanced Transportation Technologies (BATT) Program.

■ REFERENCES

(1) Kang, B.; Ceder, G. *J. Electrochem. Soc.* **2010**, *157*, A808.

(2) Li, G.; Azuma, H.; Tohda, M. *J. Electrochem. Soc.* **2002**, *149*, A743.

(3) Yamada, A.; Chung, S. *J. Electrochem. Soc.* **2001**, *148*, A960.

(4) Chen, G.; Wilcox, J. D.; Richardson, T. *J. Electrochem. Solid-State Lett.* **2008**, *11*, A190.

(5) Li, G.; Azuma, H.; Tohda, M. *Electrochem. Solid-State Lett.* **2002**, *5*, A135.

(6) Yamada, A.; Hosoy, M.; Chung, S. C.; Kudo, Y.; Hinokum, K.; Liu, K. Y.; Nish, Y. *J. Power Sources* **2003**, *232*, 119−121.

(7) Kwon, N.; Drezen, T.; Exnar, I.; Teerlinck, I.; Isono, M.; Graetzel, M. *Electrochem. Solid-State Lett.* **2006**, *9*, A277.

(8) Kim, T. R.; Kim, D. H.; Ryu, H. W.; Moon, J. H.; Lee, J. H.; Boo, S.; Kim, J. *J. Phys. Chem. Solids* **2007**, *68*, 1203.

(9) Xiao, J.; Xu, W.; Choi, D.; Zhang, J. *J. Electrochem. Soc.* **2010**, *157*, A142.

(10) Padhi, A. K.; Nanjundaswamy, K. S.; Goodenough, J. B. *J. Electrochem. Soc.* **1997**, *144*, 4.

(11) Dimesso, L.; Förster, C.; Jaegermann, W.; Khanderi, J. P.; Tempel, H.; Popp, A.; Engstler, J.; Schneider, J. J.; Sarapulova, A.; Mikhailova, D.; Schmitt, L. A.; Oswald, S.; Ehrenberg, H. *Chem. Soc. Rev.* **2012**, *41*, 5068−5080.

(12) Zaghib, K.; Mauger, A.; Julien, C. M. *J. Solid State Electrochem.* **2012**, *16*, 835−845.

(13) Jang, I. C.; Lim, H. H.; Lee, S. B.; Kartikeyan, K.; Aravindan, V.; Kang, K. S.; Yoon, W. S.; Cho, W. I.; Lee, Y. S. *J. Alloys Compd.* **2010**, *497*, 321−324.

(14) Yamada, A.; Kudo, Y.; Liu, K. Y. *J. Electrochem. Soc.* **2001**, *148*, A747−A754.

(15) Wolfenstine, J.; Allen, J. *J. Power Sources* **2004**, *136*, 150.

(16) Qin, Z.; Zhou, X.; Xia, Y.; Tang, C.; Liu, Z. *J. Mater. Chem.* **2012**, *22*, 21144.

(17) Ong, S.; Chevrier, V.; Ceder, G. *Phys. Rev. B* **2011**, *83*, 075112 S.

(18) Shang, S. L.; Wang, Y.; Mei, Z. G.; Hui, X. D.; Liu, Z. K. *J. Mater. Chem.* **2012**, *22*, 1142−1149.

(19) Oh, S. M.; Oh, S. W.; Yoon, C. S.; Scrosati, B.; Amine, K.; Sun, Y. K. *Adv. Funct. Mater.* **2010**, *20*, 3260−3265.

(20) Fang, H. S.; Yi, H. H.; Hu, C. L.; Yang, B.; Yao, Y. C.; Ma, W. H.; Dai, Y. N. *Electrochim. Acta* **2012**, *71*, 266−269.

(21) Zhang, Y. R.; Zhao, Y. Y.; Deng, L. *Ionics* **2012**, *18*, 573−578.

(22) Zaghib, K.; Trudeau, M.; Guerfi, A.; Trottier, J.; Mauger, A.; Veillete, R.; Julien, C. M. *J. Power Sources* **2012**, *204*, 177−181.

(23) Yoshida, J.; Stark, M.; Holzbock, J.; Hüsing, N.; Nakanishi, S.; Iba, H.; Abe, H.; Naito, M. *J. Power Sources* **2013**, *226*, 122−126.

(24) Liu, S.; Fang, H. S.; Yang, B.; Yao, Y. C.; Ma, W. H.; Dai, Y. N. *J. Power Sources* **2013**, *230*, 267−270.

(25) Drezen, T.; Kwon, N. H.; Bowe, P.; Teerlinvk, I.; Isono, M.; Exnar, I. *J. Power Sources* **2007**, *174*, 949−953.

(26) Rangappa, D.; Sone, K.; Zhou, Y.; Kudo, T.; Honma, I. *J. Mater. Chem.* **2011**, *21*, 15813−15818.

(27) Wang, F.; Yang, J.; Gao, P.; Nuli, Y.; Wang, J. *J. Power Sources* **2011**, *196*, 10258−10262.

(28) Liu, J.; Liu, X.; Huang, T.; Yu, A. *J. Power Sources* **2013**, *229*, 203−209.

(29) Wang, D.; Ouyang, C.; Drezen, T.; Exanar, I.; Kay, A. *J. Electrochem. Soc.* **2010**, *157*, A225−A229.

(30) Lee, J. W.; Park, M. S.; Anass, B.; Park, J. H.; Paik, M. S.; Doo, S. G. *Electrochim. Acta* **2010**, *55*, 4162−4169.

(31) Ni, J.; Gao, L. *J. Power Sources* **2011**, *196*, 6498−6501.

(32) Yang, G.; Ni, H.; Liu, H.; Gao, P.; Ji, H.; Roy, S.; Pinto, J.; Jiang, X. *J. Power Sources* **2011**, *196*, 4747−4755.

(33) Dimesso, L.; Förster, C.; Jaegermann, W.; Khanderi, J. P.; Tempel, H.; Popp, A.; Engstler, J.; Schneider, J. J.; Sarapulova, A.; Mikhailova, D.; Schmitt, L. A.; Oswald, S.; Ehrenberg, H. *Chem. Soc. Rev.* **2012**, *41*, 5068−5080.

(34) Ravnsbaek, D. B.; Xiang, K.; Xing, W.; Borkiewicz, O. N. J.; Wiaderek, K. M.; Gionet, P.; Chapman, K. W.; Chupas, P. J.; Chiang, Y. M. *Nano Lett.* **2014**, *14*, 1494−1491.

(35) Zhang, K.; Han, X.; Hu, Z.; Zhang, X.; Tao, Z.; Chen, J. *Chem. Soc. Rev.* **2015**, DOI: 10.1039/c4cs00218k.

(36) Wang, H. L.; Yang, Y.; Liang, Y. Y.; Cui, L. F.; Casalongue, H. S.; Li, Y. G.; Hong, G. S.; Cui, Y.; Dai, H. J. *Angew. Chem.* **2011**, *50*, 7364−7368.

(37) Oh, S. M.; Jung, H. G.; Yoon, C. S.; Myung, S. T.; Chen, Z. H.; Amine, K.; Sun, Y. K. *J. Power Sources* **2011**, *196*, 6924−6928.

(38) Tan, Z.; Gao, P.; Cheng, F. Q.; Luo, H. J.; Chen, J. T.; Zhou, H. H.; Tan, S. T. *Funct. Mater. Lett.* **2011**, *4*, 299−303.

(39) Damen, L.; Giorgio, F. D.; Monaco, S.; Veronesi, F.; Mastrangostino, M. *J. Power Sources* **2012**, *218*, 250−253.

(40) Von Hagen, R.; Lorrman, H.; Müller, K. C.; Mathur, S. *Angew. Chem.* **2012**, *2*, 553−559.

(41) Zong, J.; Peng, Q. W.; Yu, J. P.; Liu, X. J. *J. Power Sources* **2013**, *228*, 214−219.

(42) Yang, G.; Ni, H.; Liu, H.; Gao, P.; Ji, H.; Roy, S. *J. Power Sources* **2011**, *196*, 4747−4755.

(43) Zhang, Y.; Zhao, Y.; Deng, L. *Ionics* **2012**, *18*, 573−578.

(44) Minakshi, M.; Kandhasamy, S. *Curr. Opin. Solid State Mater. Sci.* **2012**, *16*, 163−167.

(45) Ni, J.; Gao, L. *J. Power Sources* **2011**, *196*, 6498−6501.

(46) Iturrondobeitia, A.; Goñi, A.; Palomares, V.; Gil de Muro, I.; Lezama, L.; Rojo, T. *J. Power Sources* **2012**, *216*, 482.

(47) Rodríguez-Carvajal, J. *Phys. B* **1993**, *192*, 55.

(48) Doyle, M.; Newman, J.; Reimers, J. *J. Power Sources* **1994**, *52*, 211.

(49) Palomares, V.; Goñi, A.; Gil de Muro, I.; De Meatza, I.; Bengoechea, M.; Cantero, I.; Rojo, T. *J. Electrochem. Soc.* **2009**, *156* (10), A817−A821.

(50) Yang, G.; Ni, H.; Liu, H.; Gao, P.; Ji, H.; Roy, S.; Pinto, J.; Jiang, X. *J. Power Sources* **2011**, *196*, 4747−4755.

(51) Piper, L. F. J.; Quackenbush, N. F.; Sallis, S.; Scalon, D. O.; Watson, G. W.; Nam, K.-W.; Yang, X.-Q.; Smith, K. E.; Omenya, F.; Chernova, N. A.; Whittingham, M. S. *J. Phys. Chem. C* **2013**, *117*, 10383−10396.

(52) Santoro, R. P.; Newham, R. E. *Acta Crystallogr.* **1967**, *22*, 344−347.

(53) Iturrondobeitia, A.; Goñi, A.; Lezama, L.; Kim, C.; Doeff, M.; Cabana, J.; Rojo, T. *J. Mater. Chem. A* **2013**, *1*, 10857−10862.